Supplementary information for

The duo roles of functional groups in the photoluminescence of graphene quantum dots

Shujun Wang[1,2], Ivan S. Cole[3] , Dongyuan Zhao[4], and Qin Li[1,2]*

1. Queensland Miro- and Nanotechnology Centre, Griffith University, Nathan Campus, Brisbane, QLD 4111, Australia

2. School of Engineering (Environmental), Griffith University, Nathan Campus, Brisbane, QLD 4111, Australia

3. CSIRO Materials Science and Engineering, –Gate 5, Normanby Road, Clayton, VIC 3168, Australia

4. Department of Chemistry & Laboratory of Advanced Materials, Fudan University, Shanghai, 200433, P.R. China

1. As synthesized GQDs

Carbon black (CB, Fig. S1 a), is composed of randomly oriented layered sp^2 structures (graphitic structure, Fig. S1 b) of only several nano meters in size [1, 2]. Upon the treatment in the mixed acids, CB particles were dismantled releasing the graphitic crystallites. The graphitic crystallites were further exfoliated into GQDs (Fig. S1 c). By varying the reaction time, GQDs of different sizes were obtained as confirmed by Raman spectra, dynamic light scattering (DLS) and HRTEM profile analysis.

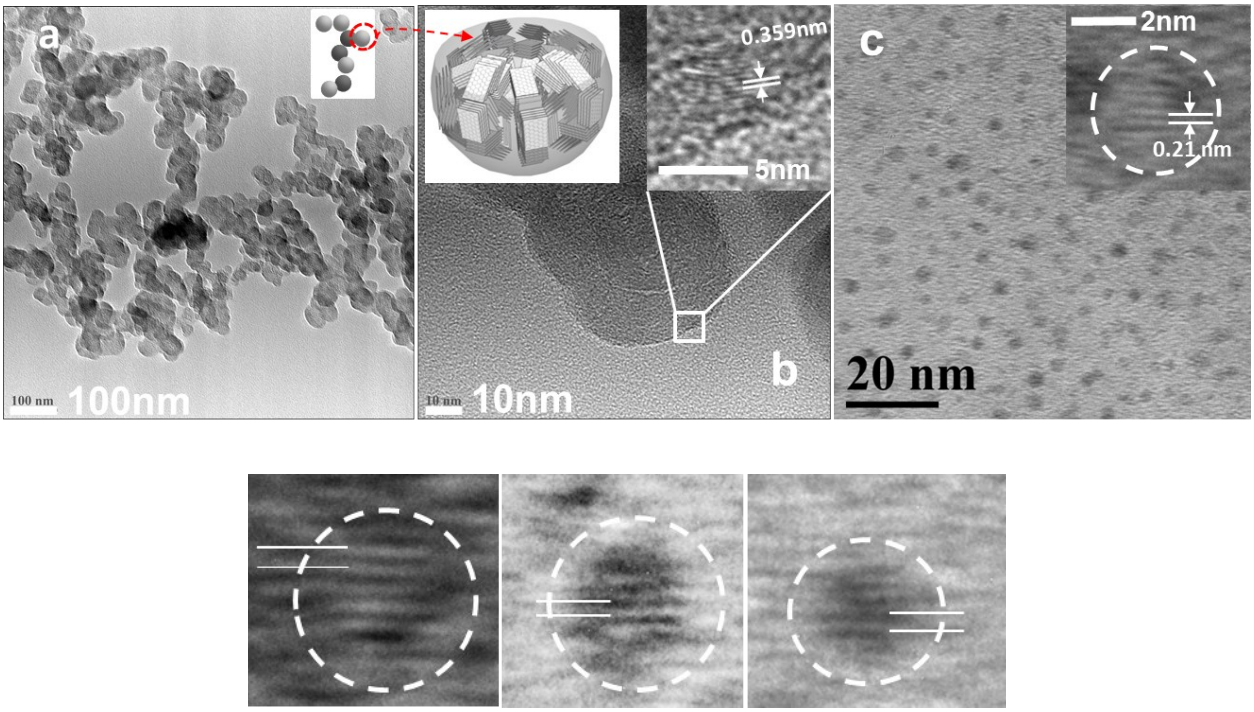

Figure S1. Morphology of CB and GQDs: HRTEM images of CB under a low magnification (a) and high magnification (b), insets are schematic representation of the sphere network and micro-structure of each sphere, respectively; HRTEM image of G20 (c), images in the second row are HRTEM images of individual dots from G20 sample showing crystal fringes, the distance between the parallel markers are all ~ 0.21nm;

The dimensions of crystallites in carbon black were derived by two techniques, namely X-ray diffraction (XRD) and Raman spectroscopy. From XRD by using the well-known Scherrer

equation[1, 3, 4] the crystallite dimension along the stacking direction (thickness of the crystallites) could be derived.

$$L_c=K\lambda/\beta\cos\Theta \quad (S1)$$

Where, K is a constant and for carbon black the value is 0.89; λ is the wavelength of X-Ray since Cu Kα X-Ray is used, λ=1.54A; β is the full width at half maximum intensity (FWHM) of the diffraction peak. Θ is half the Bragg angle. Both units of β and Θ in the formula are Radians.

Figure S2 a presents one of the XRD spectrum collected for CB employed in this study. The parameters for Equation S1 are obtain via spectrum fitting with the software Highscore Plus. By applying Equation S1 on diffraction peak of 002, the L_c for the spectrum as shown could be calculated as follow Lc=0.89X0.154/((0.073)*cos(0.217))=1.915 (nm), such a length could be translated into 5~6 layers of carbon atoms.

The in plane dimension (basal plane size) of the crystallite was calculation through applying the Tuinstra-Koenig relationship (Eq.S2) in which Raman spectra are utilized[5]. Figure S2 b is one of the Raman spectrum acquired from the CB.

$$L_a=4.35/(I_D/I_G) \quad (S2)$$

Where, I_D and I_G are the intensity of D and G bands of the Raman spectrum respectively.All the parameters used in Eq.S2 are obtained through spectra fitting with software WiRE.3.

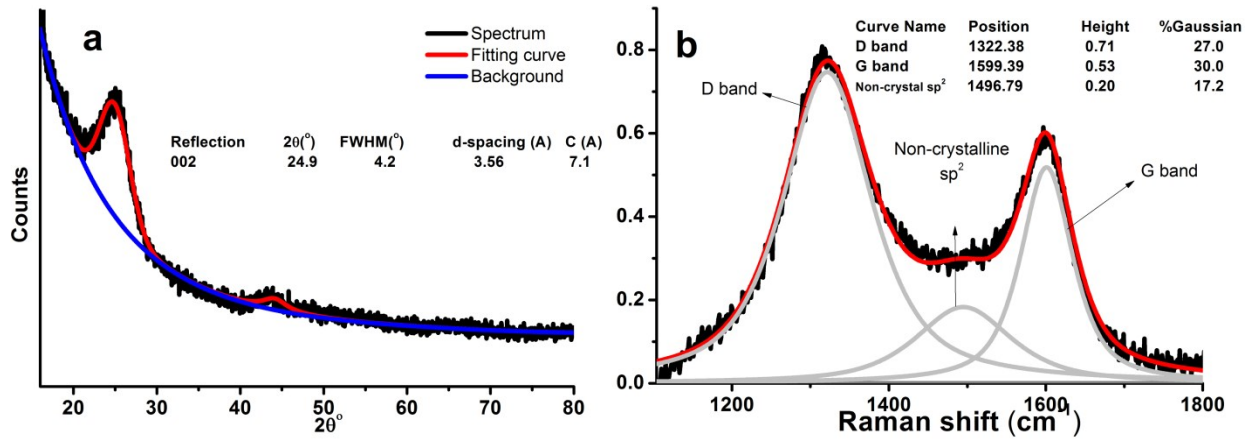

Figure S2. XRD and Raman spectra for CB employed in this research

For the size of GQDs, since they are free sp^2 crystallites exfoliated from CB, the La derived from Raman could be regarded as their particle size. The size has been reduced from ~2nm of G20 to ~1nm of G210 gradually without any abrupt change. Moreover, the sizes of as-synthesized GQDs were also confirmed by the dynamic light scattering (DLS), which agree well with the Raman analysis (Fig. S3). Besides, the size of G20 derived from TEM is around 2.3nm,

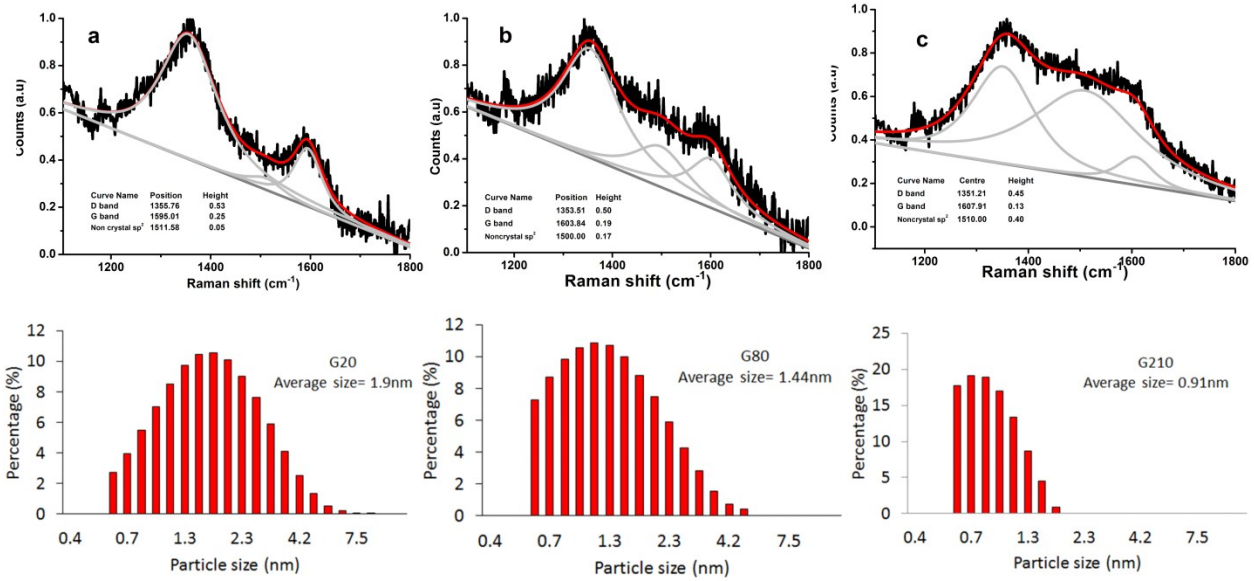

Figure S3. Raman profile fitting and DLS data: (a), G20; (b), G80; (c), G210; no DLS data could be collected below the machine limit at 0.6nm

again consistent with the Raman analysis (Fig. S4). The average thicknesses of the as synthesized GQDs are all about 1.2nm which could be translated into one or two layers of carbon atoms (Fig. S5). The as synthesized GQDs could be dispersed in water to form very stable dispersions (Fig. S6).

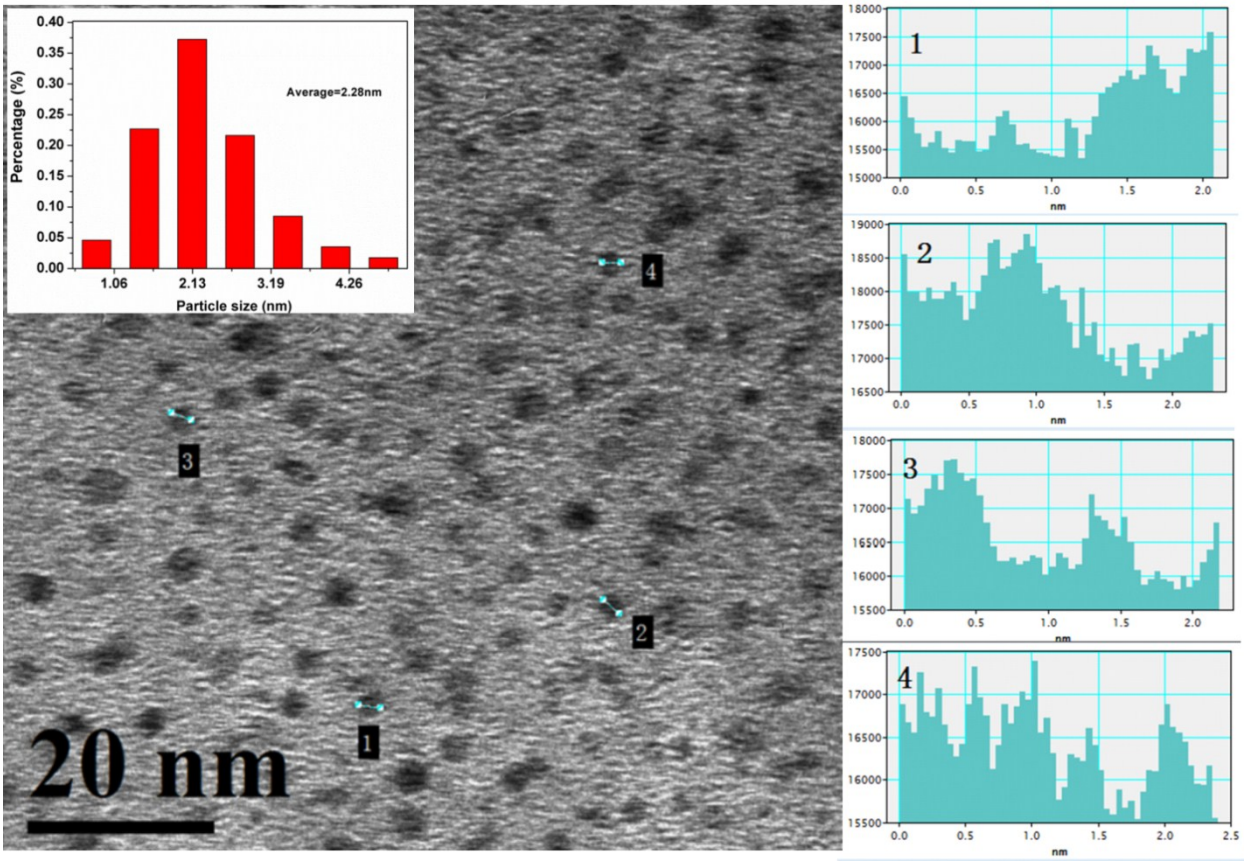

Figure S4. TEM profile analysis for G20

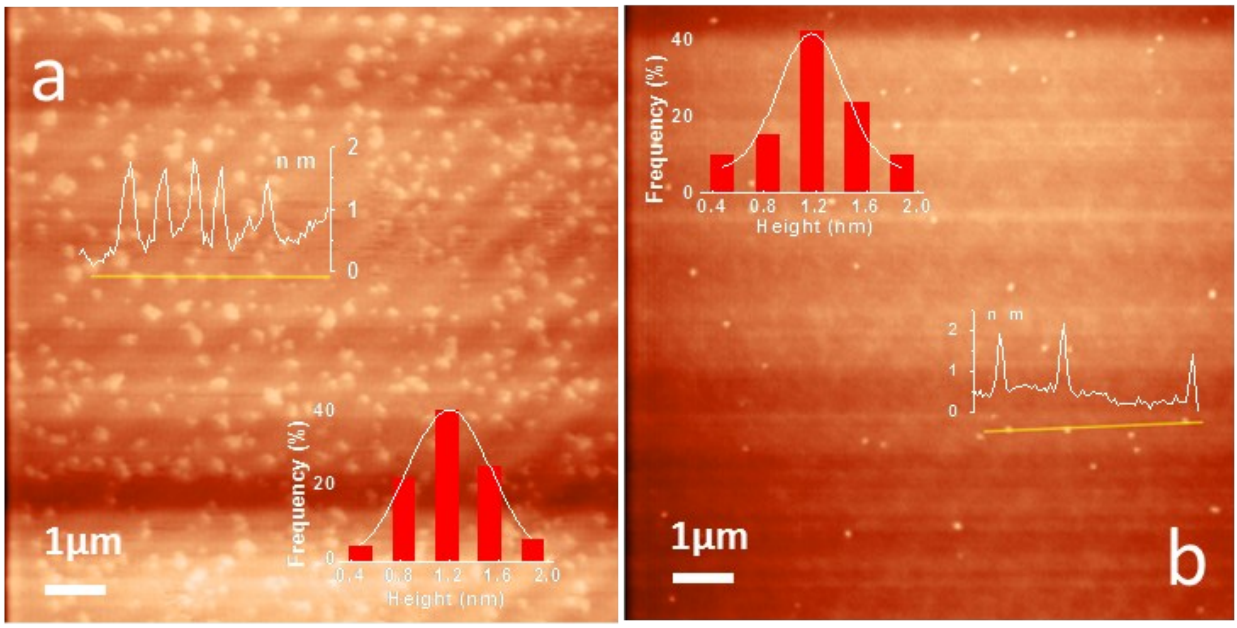

Figure S5. AFM images of GQDs: (a) G20; (b) G210. Inserted are the height profiles. Each of the height distributions were based on height profile of over 300 dots.

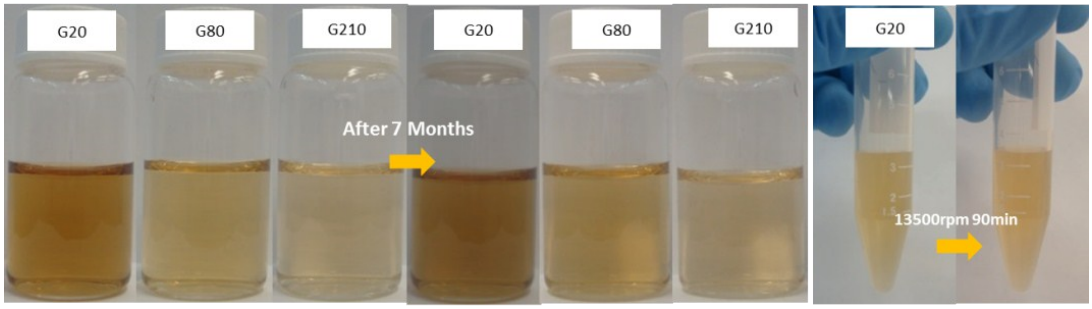

Figure S6. Stability tests of the as synthesized GQDs dispersions

2. Chemical composition analysis via XPS and FTIR

Figure S7 is the XPS spectra measured for G20, G80, G210 and the corresponding chemically reduced samples rG20, rG80 and rG210. Typical oxygen containing functional groups, namely C-O (for hydroxyl and epoxy) and C=O (for carboxyl and carbonyl) represented by each of the Gaussion-Lorentzian components (Guassion%=30%) were identified as shown in the figure. The relative atomic assignment of each functional group was summarized in Table S1. The FTIR spectra also indicate the presence of similar oxygen functional groups in the GQDs as

synthesized (Fig.S8). According to the XPS characterization, the as synthesized GQDs contain similar carbon to oxygen ratio close to 3, however, the percentages of different functional groups for the GQDs obtained at different reaction time is different (Table S1), which indicates inter-conversion of functional groups. We reckon our synthesis method follows an edge-etching mechanism. As previous studies have shown, nano-scaled graphene possess much higher chemical reactivity around edge than on the inner plane[46,47], in our strong oxidation reaction with a starting material of dismantled and exfoliated carbon black (i.e. crystallites with lateral size ~3nm), it is the atoms on the edge of GQDs that are continuously etched away, thereby reducing the size of particle in a quasi-continuous manner. The edge-etching process involves introduction and inter-conversion of the oxygenated functional groups on the GQDs edge (e.g. converting –OH into C=O or –COOH) and furthered by fully oxidation of the edge carbon atoms into CO_2 (i.e. converting C=O and –COOH into CO_2, as illustrated by the Schematic in Figure S9.

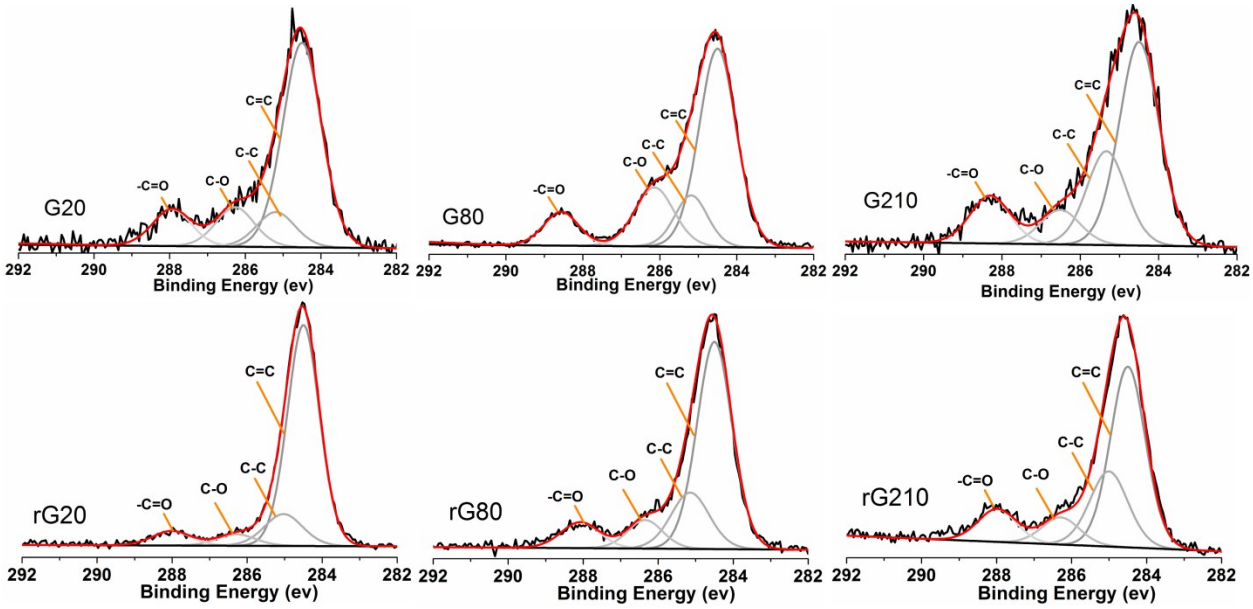

Figure S7. XPS profile fitting

Table S1. Atomic assignment

Sample	C : O	C=C	C-C	C-O	C=O
G20	3.0	64.8	11.1	12.5	11.7
G80	2.9	58.8	13.4	18.5	9.4
G210	3.2	53.7	24.6	9.1	12.6
rG20	6.6	76.3	13.1	4.7	5.9
rG80	4.2	63.7	18.9	8.8	8.7
rG210	3.6	55.1	25.0	8.9	10.9

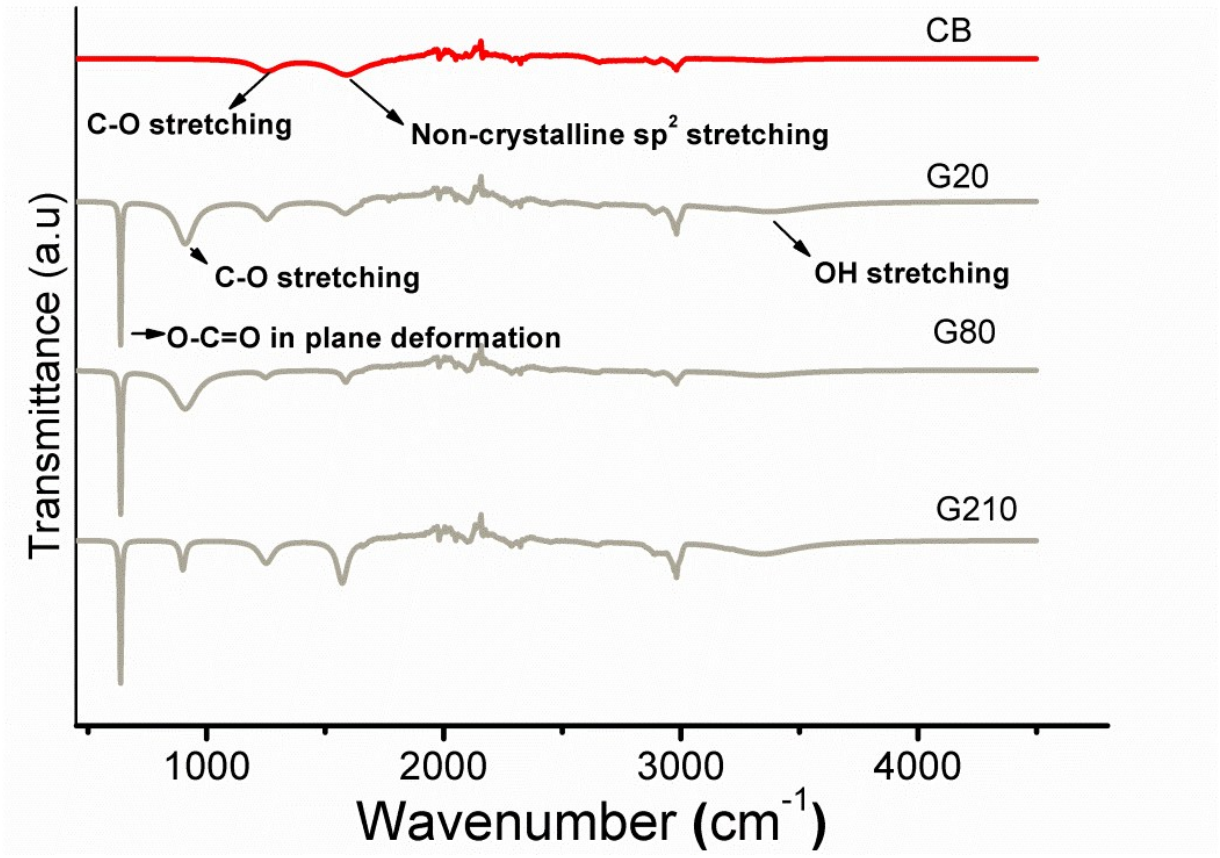

Figure S8. FTIR spectra

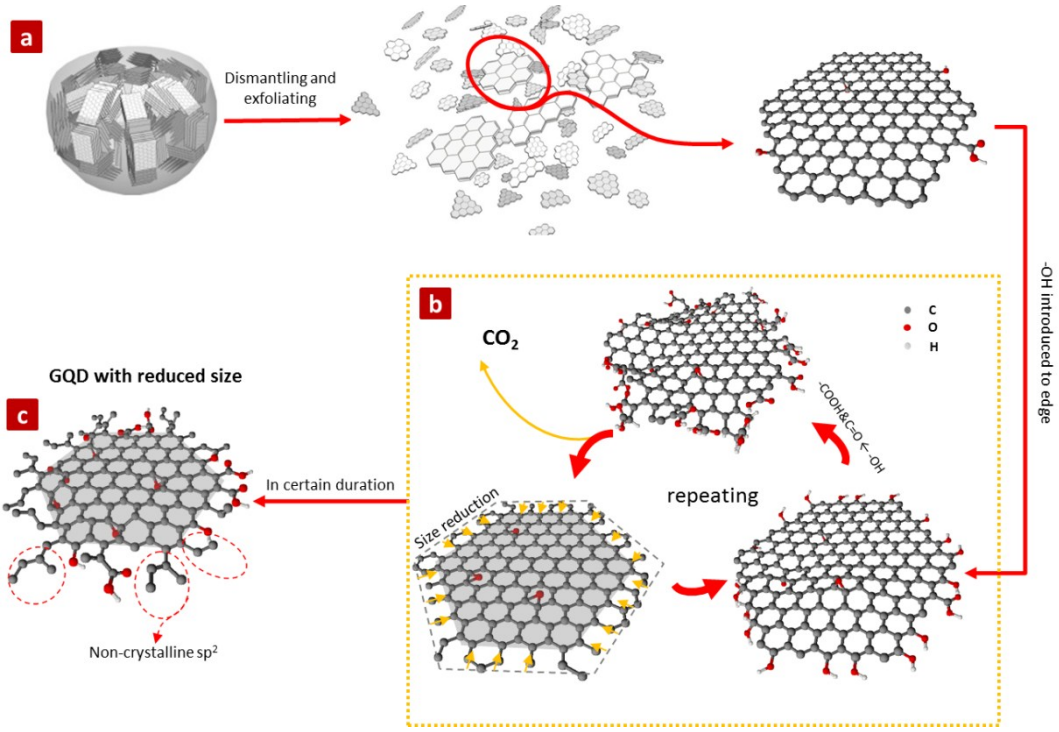

Figure S9. Schematic representation of the mechanism by which the high tuneability of size is realized: a) dismantling and exfoliation of CB into GQDs of original size; b), the oxidative environment firstly introduces hydroxyl to the edge of GQDs further convert hydroxyl into carboxyl and eventually removes peripheral carbon atoms via turning carboxyl into carbon dioxide; c) With the reaction described in b repeating overtime, the size of GQD is gradually reduced thereby widening the size.

3. The light absorption feature of GQDs

The light absorption feature of as synthesized GQDs in this study were evaluated via two techniques, namely, PLE and UV/vis. Figure S10 shows the PLE spectra of G20, G80 and G210 collected under various emission wavelengths. The spectrum becomes increasingly polarized to the left with the decrease of particle size from G20 to G210. The narrowing of the PLE spectrum is consistent with the change of size distribution as revealed by the DLS measurement (Fig. S3). It should be an indication of quantum confinement. Moreover, all three PLE spectra of G20, G80 and G210 possess a strong excitation edge at the blue side whose approximate position

(240nm~325nm) does not change with GQDs size. Such an invariable excitation edge is highly likely due to the electron transitions of the functional groups (i.e. n-σ* andn-π*).

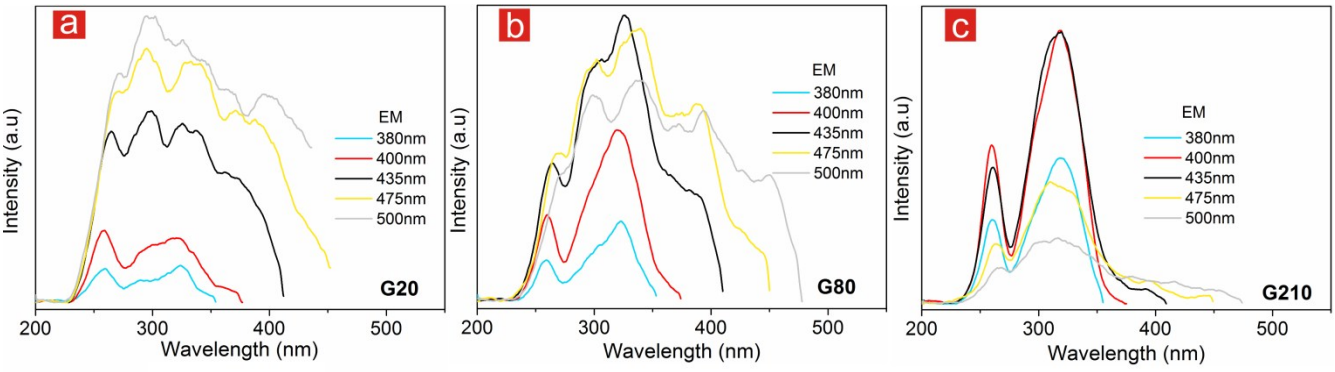

Figure S10. The PLE spectra of G20, G80, and G210

Figure S11 presents the normalized UV/Vis spectra of the as synthesized GQDs. Four absorption bands at 202, 220, 260 and 285 nm which do not spectrally change while varying the GQD size could be observed (corresponds to the absorption edge (i.e. 240~325nm) in the PLE spectrum). Similar position-fixed absorption bands were also observed in the GQDs synthesized from a bottom-up approach [6]. Moreover, we can observe a gradual reduction of the right side of the tails and rising and broadening of the left side of the tail producing a blue shifting feature of the tails as indicated by the arrow in Figure S11 a. The exact trend could be made clear by fitting the spectra. Including the four identified fixed peaks, nine components were applied to fit each of the spectra (i.e. five variable components). A clear peak intensity migration trend was identified for the five variable components, namely, the highest intensity among the five components presents a clear 'migrating' trend to the blue side (as indicated by the arrow in Fig. S11 b). Since the size of GQDs were gradually reduced from G20 to G210 as discussed in last section, it is highly likely that the 'migrating' components of the UV/Vis spectra are the result of the electron transitions from π to π* of the GQD carbon frameworks which are determined by quantum

confinement[7, 8]. The fact that it requires five components to spectrally cover this size-dependent absorbance is due to the inherent poly-dispersity of sizes of as-synthesized GQDs. In contrast, the absorption peaks possessing fixed energy absorption on the spectra, are most likely attributed to electronic transitions of functional groups (i.e. n-σ* and n-π*).

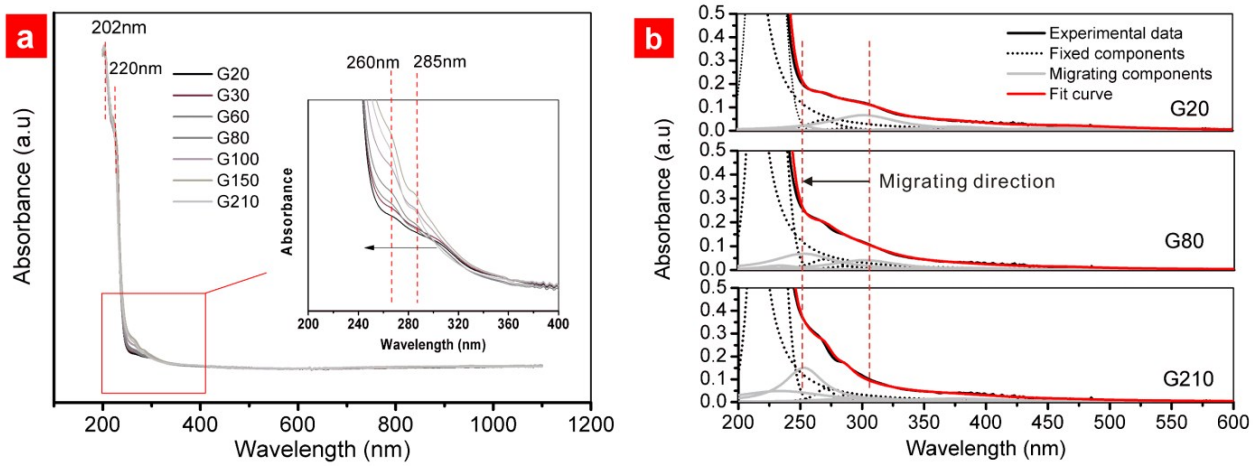

Figure S11. UV/Vis spectra of GQDs: (a) normalized spectra of GQDs synthesized for different duration (inserted is the zoom-in graph of the highlighted part of the full spectra); (b) spectra fitting for G20, G80 and G210.

3. TCSPC measurement

The TCSPC spectra were acquired on a fluorescence spectrometer (Edinburgh Photonics FLS920) with 372nm and 443nm pulse laser excitation source. The TCSPC spectra for each excitation energy were then collected at a series emissions althrough the static PL spectra as listed in the main manuscript. Figure S12 is an example of the as collected TCSPC spectra. All the TCSPC spectra could be well fitted by three exponential components as depicted by Equation S3. Table S2 presents the fitting results for TCSPC given in Figure S12. The fractions of the lifetime components τ1~ τ3 for G20, G210 and their chemically reduced counterparts rG20, rG210 under both 377nm and 443nm excitations are summarized in Figure S13.

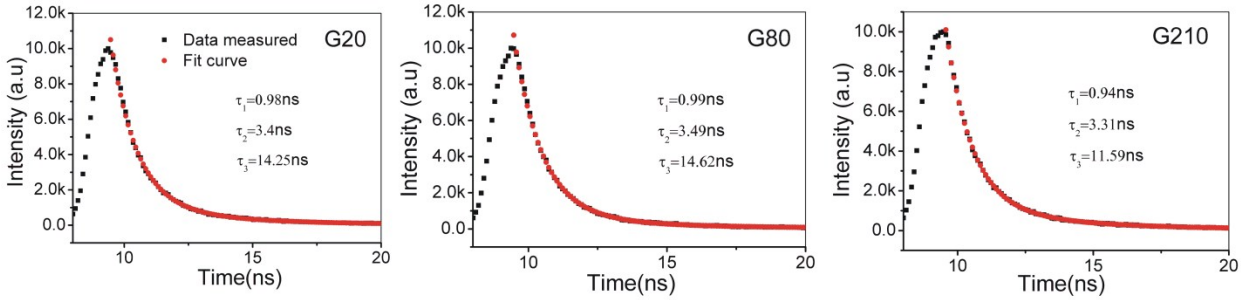

Figure S12. TCSPC spectra of GQDs collected at emission of 470nm under 372nm excitation

$$Fit = A + B_1 \cdot e^{-t/\tau_1} + B_2 \cdot e^{-t/\tau_2} + B_3 \cdot e^{-t/\tau_3} \quad \text{(S3)}$$

Where, A, B_1, B_2, B_3 are constants; τ_1, τ_2, τ_3 are the life time components.

Table S2. Summary of fitting results for TCSPC spectra as shown in Figure S9

	G20		G80		G210	
	Value (ns)	Fraction (%)	Value (ns)	Fraction (%)	Value (ns)	Fraction (%)
τ_1	0.98	64.92	0.99	72.42	0.94	59.35
τ_2	3.40	30.81	3.49	22.71	3.31	29.87
τ_3	14.25	4.27	14.62	4.87	11.59	10.78
A	15.67		15.13		17.4	
B_1	10099.15		10733.59		9594.96	
B_2	1375.77		953.79		1369.12	
B_3	45.51		48.77		141.00	
χ^2	1.19		1.18		1.02	

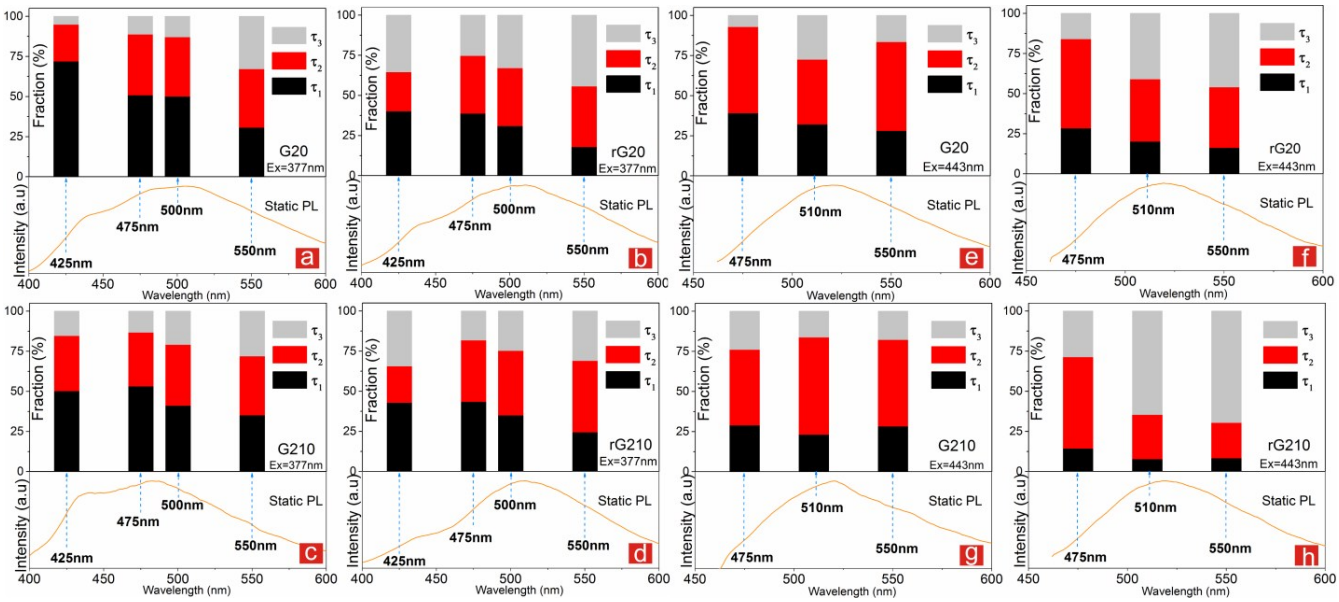

Figure S13. Lifetime components from TCSPC fitting for G20, rG20, G210 and rG210 under 377nm excitation (a-d) and 443 excitation (e-h) respectively

4. PH dependence of PL

Figure S14 shows the PL of G20, G80 and G210 under different pH values. The PL is quenched when the pH deviates from neutral for all of the three GQDs.

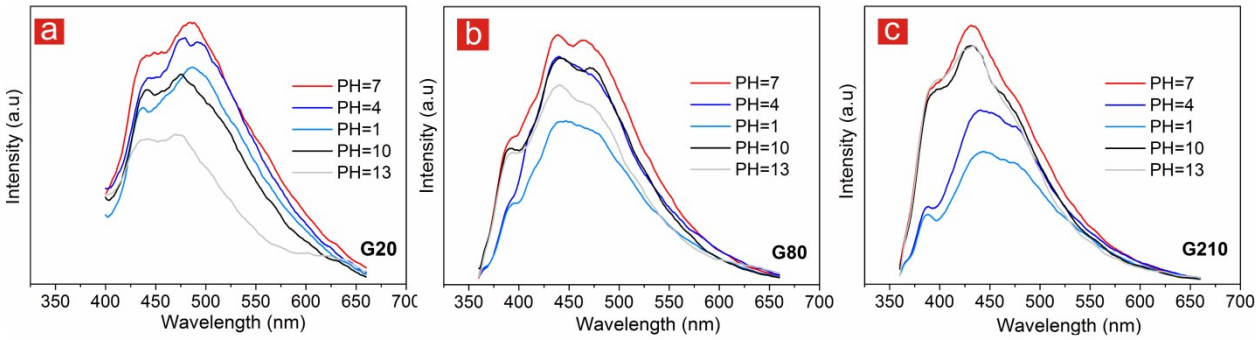

Figure S14. PL of G20, G80, G210 at different pH values

5. Details of theoretical calculation

The models of oGQDs constructed containing similar C/O atomic ratios as the GQDs synthesized in this research (~3) The density functional theory calculations were conducted with the ABINIT codes[9] (Version 7.4.3). The exchange-correlation functional adopted was localized density approximation (LDA). Norm-conserving pseudo-potentials of Troullier-Martins type

were applied. Each model of the pristine GQDs (pGQDs), disordered GQD (dGQD) and oxidized GQDs (oGQDs) was firstly relaxed via the Broyden-Fletcher-Goldfarb-Shanno minimization (BFGS) process. Following the structural relaxation, convergence studies were firstly performed on the cut-off energy to ensure selecting the proper number of plane waves and then on the size of super cell to ensure that the impact of the periodical images on the final calculation was minimized by an appropriate super cell that introduce sufficient vacuum along each of the axis. The chosen cut-off energy and super cell from the convergence studies for each of the model are listed in Table S3. The smeared density of states (DOS) were calculated with a smearing energy 0.0025Ha (0.07eV). Figure S15 is the calculation results for the 12 ring GQDs (both pGQD and oGQD). Similar to the 7 ring case in the main manuscript, there were additional energy states appeared on the oGQD energy level diagram as marked by the dark lines.

Table S3. Cut-off energies and sizes of super cells used for DFT calculation

Model	Cut-off energy (Ha)	Cut-off energy (eV)	Super cell (Bohr)
pGQD (7 rings)	25	680	(a, b, c)=(22, 22, 15)
oGQD (7 rings)	30	816	(a, b, c)=(25, 25, 15)
dGQD (7 rings)	30	816	(a, b, c)=(25, 25, 15)
pGQD (12 rings)	25	680	(a, b, c)=(25, 25, 15)
oGQD (12 rings)	30	816	(a, b, c)=(32, 32, 16)

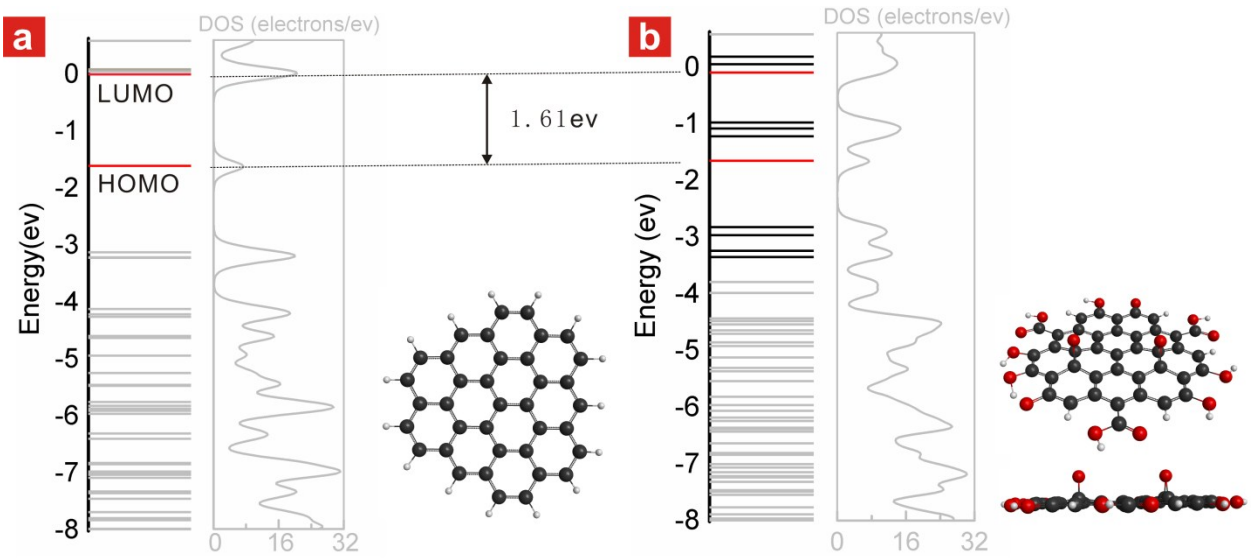

Figure S15. Energy level diagrams and DOS curves from the DFT calculation of pGQDs (a) and oGQDs (b) containing 12 benzene rings

After DFT calculation, the Maximal Localized Wannier Functions (MLWF) were extracted by Wannier90 [10](used as a library of the ABINIT codes) for three 7 rings GQD models. MLWFs are the solid state equivalent of the Boys' Functions used in chemistry for representation of molecular orbitals[11]. For a typical Wannier90 calculation, the Wannier Functions were firstly constructed with the Bloch states derived from DFT calculation and then localized through unitary transformation procedures[12, 13]. By applying two energy windows (i.e. the outer window and the frozen window), MLWFs for the targeted energy states could be extracted. For visualization of the isosurfaces, isovalue 3 is adopted for clear reveal of the hybridization conditions . Figure S16 presents the MLWFs of HOMO of pGQD and oGQD, they are all naturally hybridized π orbitals (i.e. hybridization of π orbitals along the edge of the benzene rings). Figure S17 is a schematic representation of one possible electron transition path way with the energy states induced by structural distortion (ESiD). In particular, the structural distortion

bends the benzene ring causing irregular hybridization of π orbitals across the ring (different from the natural case in which hybridization occur along the edge of the ring), such irregular hybridized π orbitals possess energy levels in between the confined π - π *band gap.

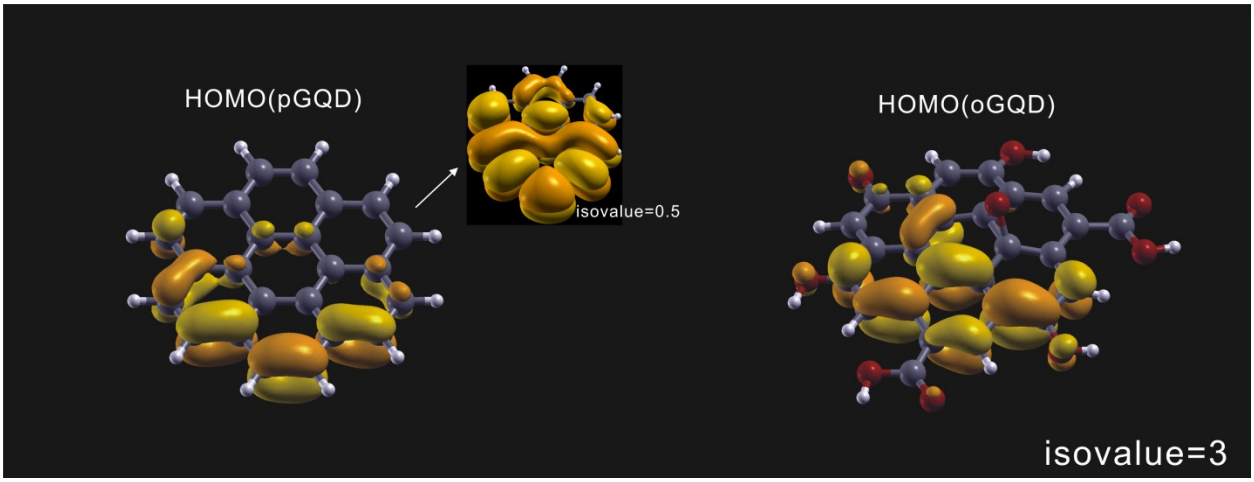

Figure S16. HOMO of pGQD and oGQD

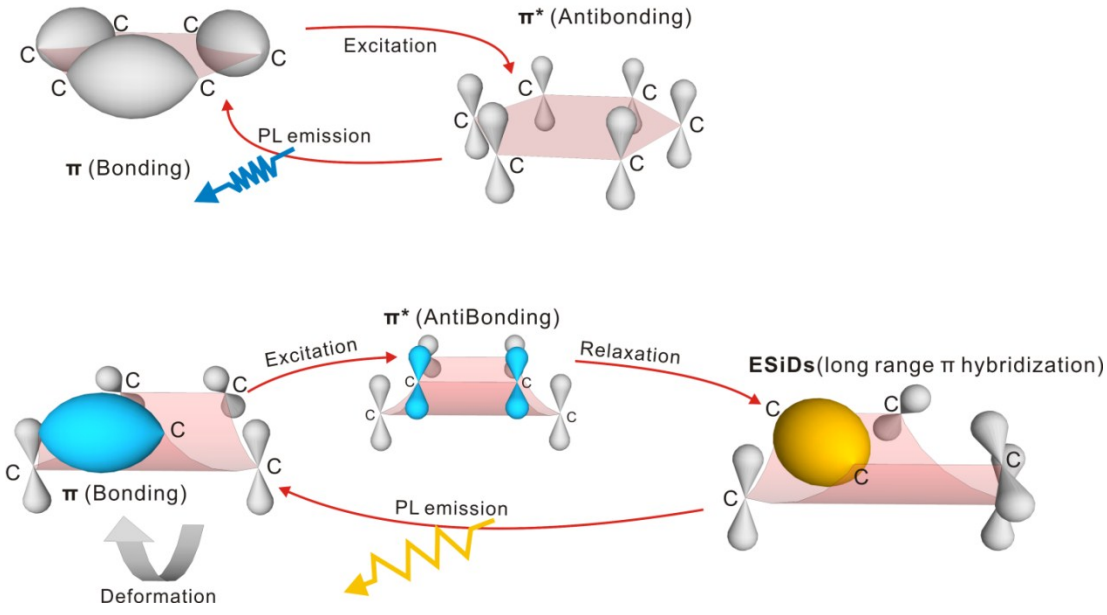

Figure S17. Schematical representation of normal π-π* transitions and one possible π-ESiD-π* transitions with ESiD as relaxation states.

Since the oxidized model discussed in the main article were constructed based on the XPS characterization of as-synthesized GQDs in this study, in order to confirm the knowledges gained in this study could be generalized to other oxygenated GQDs, we established an extra 7 ring oGQD model (shown as Model II in Fig.S18, containing 2 epoxy, 3hydroxyl, 2 carbonyl and 1 carboxyl) which has a different functional groups distribution from the model (shown as model I, containing 1 epoxy, 3 hydroxyl, 1 carbonyl and 2 carboxyl) used in the main article. Figure S18 shows the comparison among the simulation results of the pGQD, oGQD model I and oGQD

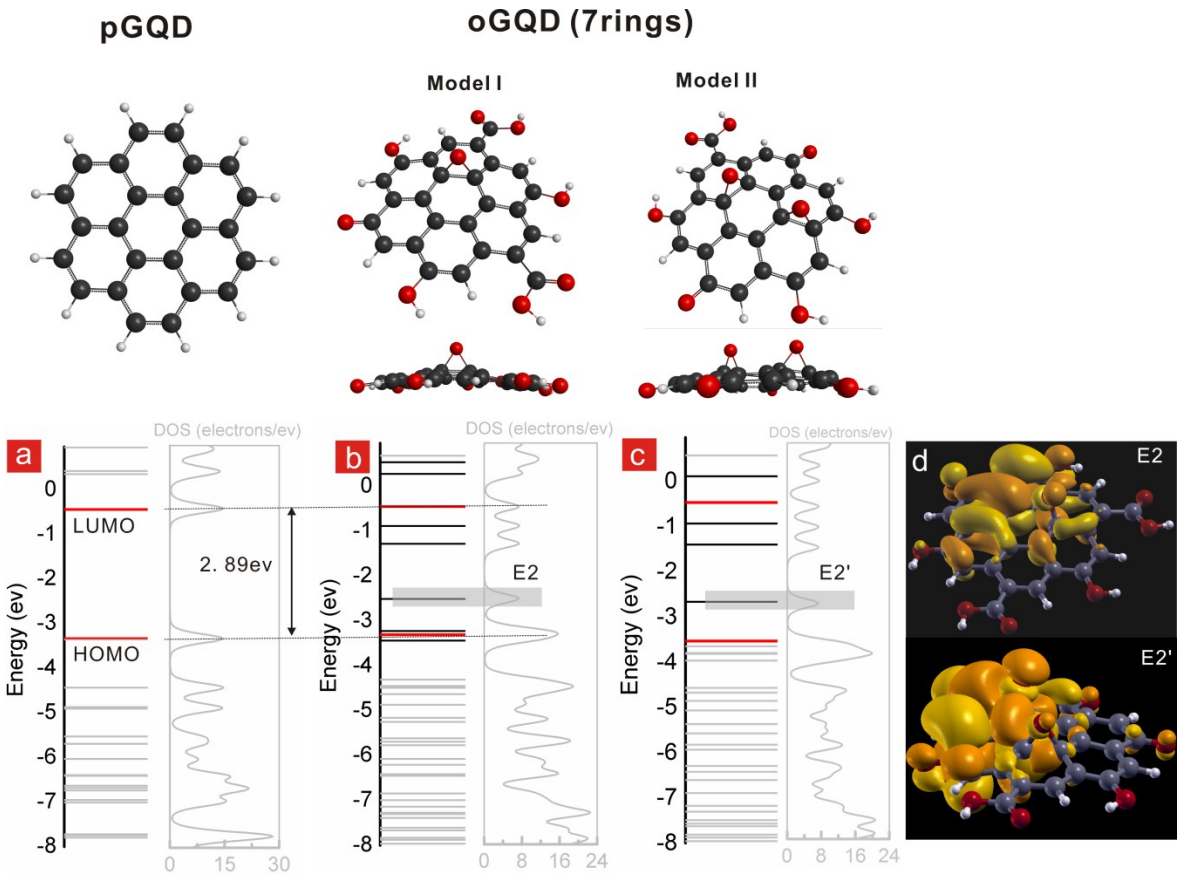

Figure S18. Comparison of simulation results of 7 rings models: a, pGQD; b, 7 ring oGQD model as discussed in main article (model I) containing 1 epoxy, 3 hydroxyl, 1 carbonyl and 2 carboxyl; c, an extra 7 ring oGQD model (model II) containing 2 epoxy, 3hydroxyl, 2 carbonyl and 1 carboxyl

model II. The calculated energy states of Model II are quite similar to model I, the similarity of electronic structures could be revealed by the energy levels diagram and especially the DOS

spectra. Moreover, the MLWFs corresponding to the typical energy level E2 (model I) and E2'(model II) also showed the similar nature of the orbitals, both containing self-orbitals of functional groups and the irregular hybridization of π orbitals. The simulation shows that the dual roles of oxygen functional groups revealed in this research are applicable to GQDs with different distribution of oxygen-containing functional groups.

Reference

1. J. Biscoe, *Journal of Applied Physics*, 1942, **13**, 364.
2. T. Ungar, J. Gubicza, G. Ribarik, C. Pantea and T. W. Zerda, *Carbon*, 2002, **40**, 929-937.
3. B. E. Warren, *Phys Rev*, 1941, **59**, 693-698.
4. A. Manivannan, M. Chirila, N. C. Giles and M. S. Seehra, *Carbon*, 1999, **37**, 1741-1747.
5. F. Tuinstra, *The Journal of Chemical Physics*, 1970, **53**, 1126.
6. L. B. Tang, R. B. Ji, X. K. Cao, J. Y. Lin, H. X. Jiang, X. M. Li, K. S. Teng, C. M. Luk, S. J. Zeng, J. H. Hao and S. P. Lau, *Acs Nano*, 2012, **6**, 5102-5110.
7. G. Eda, Y. Y. Lin, C. Mattevi, H. Yamaguchi, H. A. Chen, I. S. Chen, C. W. Chen and M. Chhowalla, *Advanced materials*, 2010, **22**, 505-509.
8. B. Mandal, S. Sarkar and P. Sarkar, *Journal of Nanoparticle Research*, 2012, **14**.
9. X. Gonze, B. Amadon, P. M. Anglade, J. M. Beuken, F. Bottin, P. Boulanger, F. Bruneval, D. Caliste, R. Caracas, M. Cote, T. Deutsch, L. Genovese, Ph. Ghosez, M. Giantomassi, S. Goedecker, D.R. Hamann, P. Hermet, F. Jollet, G. Jomard, S. Leroux, M. Mancini, S. Mazevet, M.J.T. Oliveira, G. Onida, Y. Pouillon, T. Rangel, G.-M. Rignanese, D. Sangalli, R. Shaltaf, M. Torrent, M.J. Verstraete, G. Zerah and J. W. Zwanziger, *Computer Physics Communications*, 2009, **180**, 2582-2615.
10. A. A. Mostofi, J. R. Yates, Y. S. Lee, I. Souza, D. Vanderbilt and N. Marzari, *Computer Physics Communications*, 2008, **178**, 685-699.
11. N. Marzari, A. A. Mostofi, J. R. Yates, I. Souza and D. Vanderbilt, *Rev Mod Phys*, 2012, **84**.
12. N. Marzari and D. Vanderbilt, *Phys Rev B*, 1997, **56**, 12847-12865.
13. I. Souza, N. Marzari and D. Vanderbilt, *Phys Rev B*, 2002, **65**.